Effect of wind turbulence on gas transport in porous media: Experimental method and preliminary results.

A. POURBAKHTIAR[a,b], T.G. POULSEN[b], S. WILKINSON[c] & J.W. BRIDGE[a]

[a]*School of Engineering Sciences, University of Liverpool, Liverpool L69 3BX, UK,*

[b]*Department of Civil Engineering, Xian Jiaotong-Liverpool University, Suzhou Industrial Park, 215123, Jiangsu Province, China, and*

[c]*Department of Civil Engineering, University of Wolverhampton, UK.*

Correspondence: A. Pourbakhtiar. E-mail: alirezap@liv.ac.uk

Running title: Wind-induced gas transport in porous media

Summary

We demonstrate a novel experimental arrangement for measuring wind turbulence-induced gas transport in dry porous media under controlled conditions. This equipment was applied to assess the effect of wind turbulence on gas transport (quantified as a dispersion coefficient) as a function of distance to the surface of the porous medium exposed to wind. Two different strategies for the measurement of wind-induced gas transport were compared. Experiments were carried out with O_2 and CO_2 as tracer gases with average vertical wind speeds of 0.02 to 1.06 m s^{-1}. Oxygen breakthrough curves as a function of distance to the wind-exposed surface of the porous medium were analysed numerically with a finite-difference based model to assess gas transport. We showed that wind turbulence-induced gas transport is an important transport mechanism that can be 20 to 70 times larger than molecular diffusion-induced transport. Wind conditions and properties of the porous medium had strong controlling effects on this relation. Importantly, we show that even though wind-induced gas transport is greatest near to the wind-exposed surface, it can have marked effects on the variation in gas concentration at much larger depths.

Keywords: Wind speed, porous media soil, soil–air boundary, turbulent flow, molecular diffusion, gas dispersion, breakthrough time.

Highlights

- We explored the effect of atmospheric wind turbulence on gas transport in porous media.
- We measured the depth relation of wind-induced dispersion in porous media for real wind conditions.
- Wind-induced gas dispersion coefficients were 20 to 70 times larger than molecular diffusion.
- Wind turbulence can potentially have a considerable effect on gas transport in porous media

Introduction

Greenhouse gases play in important role in global warming. Soil is a source of some greenhouse gases such as methane (CH_4), carbon dioxide (CO_2) and nitrous oxide (N_2O). Various soil properties affect soil gas emissions, such as humidity, temperature, air pressure and vegetation (Oertel *et al*., 2016). Furthermore, the emission of methane, which is an important greenhouse gas, can result from land management such as from rice paddy soil and landfill sites that receive organic matter (Topp & Pattey, 1997). Radon (Rn) is a radioactive gas that can move from soil to the atmosphere with the potential to affect human health. Advective flow controlled by wind and the difference between indoor and outdoor temperatures are the main factors in the transport process of radon from soil to air and buildings (Nazaroff, 1992). Oliver & Khayrat (2001) found that in addition to lithology,

58 factors such as elevation, soil depth and particle size can affect the spatial variation
59 in radon in the soil atmosphere. .
60 Wind action (high-frequency velocity or pressure fluctuations caused by wind
61 turbulence) has been shown in several cases to play an important role in the transport
62 of gaseous compounds in soil and other porous media, and the exchange of these
63 compounds with the atmosphere. Examples include: radon (Rn) transport into
64 buildings (Riley *et al*., 1999; Wang & Ward, 2002), landfill gas emissions (Poulsen
65 *et al.*,2001; Poulsen & Moldrup, 2006), water evaporation from soil (Hanks &
66 Woodruff, 1958; Acharya & Prihar, 1969; Ishihara *et al.*, 1992; Novak *et al*.,
67 2000a,200b) and exchange of natural soil gases with the atmosphere (Takle *et al*.,
68 2004; Massman & Frank, 2006; Maier *et al*., 2012). In particular, Poulsen &
69 Moldrup (2006) identified that wind-induced turbulence was responsible for 40% of
70 total landfill gas emissions at a Danish landfill site during a 7-day period. Hanks &
71 Woodruff (1958) found that the rate of water evaporation increased two to six times
72 for soil mulches and 10 to 15 times for gravel and straw when wind speed increased
73 from 0 to 40 km $hour^{-1}$.
74 Wind turbulence (gustiness) affects gas transport in porous media by inducing
75 high-frequency, multi-directional fluctuations in gas velocity with durations of up to
76 one minute within the pore system of the porous medium (Takle *et al*., 2003;
77 Poulsen & Moldrup, 2006; Maier *et al*., 2012). These fluctuations, in turn, result in
78 gas transport by advection and dispersion in addition to the molecular diffusion
79 which is always present (Maier *et al*., 2012).

Several studies have modelled the effect of the gustiness of wind on gas transport in porous media in one, two and three dimensions (Farrell *et al*., 1966; Scotter & Raats, 1969; Kimball & Lemon, 1970; Colbeck, 1981). These studies have generally represented wind action as sinusoidal pressure or velocity waves (including superimposed waves) to simplify computation. However, Poulsen & Moldrup (2006) used stochastic modelling to generate random fluctuations with specific statistical properties. A comparison of the modelling results from these two approaches showed that wind-induced gas transport in porous media is a multi-dimensional process, and that the use of sinusoidal functions to represent one-dimensional wind action generally underestimates gas transport. The above studies show further that wind-induced gas transport decreases with increasing distance from the surface exposed to wind action.

In general, modelling of wind-induced gas transport has been done by simulating the velocities of advective pore gas as functions of location (depth) and time within the porous medium. For real (random) wind velocity or pressure fluctuations, this is computationally intensive because very small time steps are required to resolve the fluctuations (Saffman, 1960; Poulsen & Sharma, 2011). The gustiness of wind at the surface of the porous medium generates velocities of pore gas that fluctuate rapidly in magnitude and direction (Maier *et al*. 2012). The velocities also vary spatially within the porous medium because of differences in pore size. This results in mixing of the gas within the porous medium, but does not usually generate net advective gas fluxes. This means that wind turbulence-induced gas movement in porous media behaves like a dispersive process (Poulsen & Moldrup, 2006). Computationally

intensive simulations can be avoided, therefore, by modelling wind turbulence-induced gas transport as a purely dispersive process with a cumulative location-dependent dispersion coefficient, D_{tot}, that represents the sum of molecular diffusion, D_m, and wind-induced mixing, D_w (Poulsen *et al*., 2001; Poulsen & Sharma, 2011). This approach, however, requires knowledge about the relation between D_w and distance from the surface exposed to wind. Experimental investigations of D_w are limited at present, however. The authors are aware of four earlier studies only that focus on this property. Scotter & Raats (1968, 1969) and Poulsen & Sharma (2011) measured D_w in columns of porous media under fluctuations in sinusoidal pressure induced by an oscillating piston (one-dimensional gas transport). Maier *et al*. (2012) carried out similar experiments, but used a fan combined with a chopper wheel, which is a wheel-shape frame with shutters inside to generate more realistic conditions of wind turbulence. These four studies measured gas concentrations as a function of time at both ends of the columns. None of these studies, however, assessed the variation in D_w with position inside the columns of the porous medium, but measured average D_w values only across the entire columns. Therefore, to the best of the authors' knowledge there is no experimental assessment in the scientific literature at present of the relation between D_w and distance to the surface of the porous medium exposed to the wind or the effect of column length on the dispersion coefficient. To provide such knowledge would require measurements of gas concentration at different positions within the porous medium.

This research had two main objectives, therefore. First, to measure the variation in gas concentration of the porous medium in response to wind turbulence at

different distances from the surface exposed to wind, and second to use these measurements to determine D_w as a function of distance to the surface exposed to wind. Measurements were made by two different methods: (i) gas concentrations were measured at both ends of a porous medium column, following the approach used in previous research. To assess the effect of distance, columns of different length were used with one end exposed to wind turbulence, and (ii) gas concentrations were measured at several distances from the surface exposed to wind simultaneously within the same column. The results are used to compare the two methods of measurement and to assess the relation between the wind-induced dispersion coefficient D_w and distance below the surface exposed to wind.

Theory

Gas transport in porous media is traditionally described by the advection–dispersion equation (ADE). For three-dimensional transport of a non-sorbing gas in a porous medium with no liquid phase, the ADE is given as:

$$\frac{\partial C}{\partial t} = \nabla^2(DC) - \nabla(vC), \quad (1)$$

where C is the pore gas concentration, t is time, $\underline{D}$ is the diffusion–dispersion coefficient (representing the sum of molecular diffusion and mechanical dispersion) and v is the gas velocity (Darcy velocity). In a porous medium where v is controlled solely by wind turbulence, Equation (1), there is no systematic movement of gas, but random fluctuations in velocity only. As discussed in the introduction, gas phase movement can then be expressed as a dispersive process with a cumulative diffusion–dispersion coefficient, D_{tot}, which represents the sum of molecular

147 diffusion D_m and wind-induced mixing D_w (Poulsen *et al.*, 2001; Poulsen & Sharma,
148 2011). In this case Equation (1) reduces to

$$\frac{\partial C}{\partial t} = \nabla^2(D_{\text{tot}}C). \quad (2)$$

149 For a porous medium where gas concentration and wind conditions in the
150 atmosphere at its surface exposed to wind are uniform, net gas transport in the
151 porous medium is one-dimensional (Poulsen *et al.*, 2001) and Equation (2) becomes:

$$\frac{\partial C}{\partial t} = \frac{\partial^2(D_{\text{tot}}C)}{\partial z^2} = \frac{\partial^2((D_m+D_w)C)}{\partial z^2}, \quad (3)$$

152 where z is the distance from the surface exposed to wind.

153 The coefficient of molecular diffusion in the porous medium (D_m) can be
154 estimated from the molecular diffusion coefficient in free air (D_0) with for instance
155 the Penman (1940) model,

$$\frac{D_m}{D_0} = 0.66\varepsilon\ , \quad (4)$$

156 or the Millington & Quirk (1961) model

$$\frac{D_m}{D_0} = \frac{\varepsilon^{10/3}}{\phi^2}\ , \quad (5)$$

157 where ε is gas-filled porosity and ϕ is total porosity (assumed to be equal in media
158 with no liquid phase)

159 **Materials and methods**

160 *Material characteristics*

161 The dry porous medium used in this study was a crushed and polished, sub-rounded
162 marble rock with particle sizes that ranged between 6.3 and 14 mm. This material
163 was selected because it was very permeable to gas, which allowed the effects of

164 wind turbulence to penetrate deep into the medium. This also made it easier to
165 compare the methods to measure D_w and to assess the relation between D_w and
166 distance to the surface exposed to wind.

167 Gas permeability in a porous medium, *k*, was determined by measurement of the
168 drop in pressure ΔP across a sample of the medium with length *L* and cross-sectional
169 area A_s exposed to a gas flow *Q*, followed by the application of Darcy's law
170 (Kirkham, 1947),

$$k = \frac{Q\,\eta\,L}{A_s\,\Delta P}, \quad (6)$$

171 where η is the dynamic viscosity of the gas. Darcy's law was chosen because
172 relations between *Q* and ΔP were approximately linear. Particle shape of the medium
173 was characterized by particle roundness, ρ, given as (Russ, 2007)

174 $$\rho = \frac{4\,A_p}{\pi\,R^2}, \quad (7)$$

175 where A_p is the area of a two dimensional image of the particle and *R* is the major
176 axis of the best fitting ellipse to the area, A_p of the particle image. The roundness
177 was determined by analysing images of 459 randomly selected particles with ImageJ
178 (National Institutes of Health, Bethesda, MA, USA). An overview of the physical
179 characteristics of the porous medium is given in Table 1.

180 *Experimental set-up*

181 We developed our experimental set-up based on those used by Scotter & Raats
182 (1968), (1969); Poulsen *et al*. (2008); Poulsen & Sharma (2011) and Maier *et al*.
183 (2012). It was designed to enable measurements of gas (oxygen) concentration on

184 samples of variable thickness at several locations within each sample. A schematic
185 diagram of the set-up is shown in Figure 1. It consists of a 56-cm high, 25-cm inner
186 diameter PVC column divided into two separate chambers by a perforated metal
187 plate with 1-mm holes that cover 30% of the surface of the plate. The upper chamber
188 was used to hold a porous medium sample of the desired depth. Samples with depths
189 less than the depth of the chamber were supported by an additional perforated metal
190 plate. This plate was adjustable to any elevation within the chamber so that surface
191 of the sample was level with the top of the column. A 1.5 m × 1.5 m wooden board
192 with a hole the same diameter as the column was installed horizontally, and level
193 with the top edge of the column to minimize unwanted patterns of standing wind
194 turbulence around the column. The lower chamber was connected to a pressurized
195 source of CO_2 through a precision ball flow meter, Model LZM-15ZT (Yuyao
196 Kingtai Instrument Co., Ltd, Yuyao, China). A differential pressure sensor (AB
197 Micatrone, Solna, Sweden) was connected to the lower chamber to facilitate
198 measurements of pressure gradient across the sample. The column was fitted further
199 with several KE-50 galvanic oxygen electrodes (Yuasa Power Supply Ltd, Kyoto,
200 Japan) connected to a Campbell Scientific CR 1000 data logger (Campbell
201 Scientific, Logan, UT, USA). To reduce the effects of preferential gas transport,
202 oxygen sensors were not installed directly above one another but at different
203 positions along the inner wall of the column (Figure 1 right). The column was further
204 fitted with a Gill Wind master ultrasonic anemometer (Gill Instruments Ltd.
205 Lymington, UK) for three-dimensional wind speed measurements at one second
206 intervals. The main axis of the anemometer was placed 10 cm above the surface of

207 the sample. A fan was used to create the desired wind conditions by adjusting the fan
208 speed and inclination, and also distance between the fan and column.

209 *Experimental procedure*

210 The dry porous medium was packed into the upper chamber of the column in 5-cm
211 increments to ensure a homogeneous medium. During each experiment, the column
212 was saturated initially with CO_2. Carbon dioxide was used rather than N_2 because it
213 is heavier than air, which avoids the effects of buoyancy-driven flow that occurs
214 when N_2 is used, which is lighter than air. During the saturation process, the top of
215 the column was closed with a non-air tight lid. The level of CO_2 saturation (replacing
216 the atmospheric air) was monitored by an oxygen sensor placed on top of the porous
217 medium (at saturation the sensor would read zero O_2). At saturation, the CO_2 supply
218 was switched off, the fan was turned on and the lid was removed by sliding it
219 horizontally to minimize disturbance to the gas phase inside the column during its
220 removal. Atmospheric air would then re-enter the column by molecular diffusion and
221 wind-induced mixing, and the progress of air entry was recorded by oxygen
222 electrodes at one-second intervals. Experiments were continued until oxygen
223 concentrations had reached 21% throughout the column. Room temperature was
224 recorded during all experiments. Oxygen was used as an indicator of the amount of
225 air that has entered the column.

226 Two sets of experiments (A and B) were carried out. In set A, six different
227 sample thicknesses (5, 10, 15, 20, 25 and 30 cm) were considered. These
228 experiments were carried out with one oxygen sensor at the bottom of the sample
229 and another placed in the lower chamber at 46-cm depth (to ensure full oxygen

penetration). This approach is equivalent to that used in earlier research (Scotter & Raats, 1968, 1969; Maier *et al*., 2012; Poulsen & Sharma, 2011). The experiments were carried out in triplicate for four different wind conditions (0, 3, 10 and 11 in Table 2) to give a total of 72 experiments and 144 oxygen breakthrough curves.

In all set B experiments, a sample thickness of 35.5 cm (corresponding to the height of the upper chamber) was used. In all experiments, five oxygen sensors were placed inside the sample at depths of 5.5, 13, 20.5, 28 and 35.5 cm and one sensor was placed in the lower chamber at a depth of 46 cm. This number of sensors was chosen as a 'trade-off' between accuracy in the estimates of the D_w-depth relations and the amount of computation time required to determine D_w. Set B experiments were carried out in triplicate for 13 different wind conditions (Table 2) to give a total of 39 experiments and 234 oxygen breakthrough experiments. An example of wind speed measurements for wind condition 9 is shown in Figure 2. Wind conditions were chosen based on the possible settings of the fan and to cover a reasonable range of near-surface wind speeds and turbulence intensities (represented by the standard deviation in wind speed).

Data analyses

A one-dimensional numerical model used to solve Equation (3) with an explicit forward time, central space finite difference method that was implemented in Microsoft Excel with the following initial and boundary conditions:

$$C(z,t) = 0 \qquad \text{for } z \geq 0 \text{ and } t = 0, \tag{8a}$$

$$C(z,t) = 0.21 \qquad \text{for } z = 0 \text{ and } t > 0. \tag{8b}$$

One-dimensional modelling was chosen because one measurement only was available for each depth. This is equivalent to assuming that vertical concentration gradients only existed in the column. The model was fitted to the measured oxygen concentration data to determine values of D_w as a function of sample depth for different wind conditions. For experiment A, the model fitting procedure was carried out as follows: for each wind condition, the model was fitted to the oxygen breakthrough curves for the oxygen sensors placed at the bottom of the 5-cm sample and in the lower chamber simultaneously by optimizing the values of D_{tot} in the porous medium and in the free air phase below. The model was then applied to the 10-cm depth sample assuming that D_{tot} for the top 5 cm of that sample is equal to that fitted to the 5-cm sample while optimizing the values of D_{tot} for the bottom 5 cm of the 10-cm sample and the free air phase below. This procedure was applied to samples of consecutively increasing thickness to give a D_{tot} value for each 5-cm depth increment. The approach assumes that the value of D_{tot} for a given depth is independent of the thickness of the sample. For experiment B, the model was fitted to the six oxygen concentration datasets from the oxygen sensors inside the porous medium and in the lower chamber simultaneously by optimizing D_{tot} values for each of the five depth increments represented by the sensors. Breakthrough was very rapid for shallow depths, and the corresponding values of D_w were not always physically meaningful. Therefore, the model was fitted so that D_w could not increase with depth (see Fukuda, 1955). For both sets of experiments, model fitting was done by minimizing the root-mean-square error (RMSE) between measured and fitted oxygen concentrations.

$$\mathrm{RMSE} = \sqrt{\frac{1}{n}\sum_{i=0}^{n}(C^{n}_{\mathrm{measured}} - C^{n}_{\mathrm{fitted}})^{2}}, \quad (9)$$

where n is the number of measurements of concentration. The model fitting procedure was done with Microsoft Excel. For wind condition 0, the fitted values of D_{tot} for the porous medium and the free air space correspond to the molecular diffusion coefficients D_m and D_0, respectively. For wind conditions 1–12, the fitted D_{tot} values for the porous medium correspond to $D_m + D_w$. Values of D_w are obtained by subtracting D_m from D_{tot}. Prior to the determination of D_w, all values of D_m were standardized to a temperature of 20°C based on data from Denny (1993).

Results and discussion

The observed values of D_m and D_0 were independent of depth of the porous medium, as expected, and relatively constant in their agreement with theory. Average values of D_m and D_0 at 20°C across all experiments at wind condition 0 were 0.0485 $cm^2\ s^{-1}$ with a standard deviation of 0.013 and 0.12 $cm^2\ s^{-1}$ with a standard deviation of 0.009, respectively. By comparison, values in the literature for D_0 as the binary diffusion coefficient of CO_2 and air at 20°C are about 0.16 $cm^2 s^{-1}$ according to Denny (1993). The deviation between these values might be explained partly by differences in experimental set-up and the sensors used. Estimates of D_m by Equations (4) and (5) did not compare well with the measured values, probably because these equations were developed for soil, which is much finer grained than the medium used here.

Figure 3 shows the six oxygen breakthrough curves for experiment B at wind condition 3, which corresponds to the six oxygen sensors installed inside and below the sample. Figure 3 shows the curves that represent the fitted numerical model. These show that it is possible to obtain models that fit well to the measured concentration data. This was also the case for the remaining experiments, indicating that Equation (3) can be used to describe wind-induced gas transport.

Comparison of experimental approaches for measuring wind-induced gas transport

Values of D_w for wind conditions 3, 10 and 11 for both experiments A and B are shown in Figure 4 where the D_w–z relations follow similar patterns for both types of experiments. There is a large D_w zone near the wind-exposed surface below which D_w decreases quite rapidly with depth to approximately zero. Maximum values of D_w are of the same order of magnitude in both types of experiments, however, the range of observed values is 3.5 times larger for experiment B than experiment A. For experiment A, the zone of large D_w values extends about 30% deeper on average than in experiment B.

These observations indicate that there is a difference between the two methods of measurement to represent wind-induced gas exchange. This is probably because the assumption that both the wind-induced gas transport and the value of D_w for a given depth are independent of sample thickness is not completely correct, especially for samples that are less than approximately 10-cm thick for the material used in this study. A possible explanation is that for thin samples the effects of wind turbulence can penetrate through the sample and into the gas-filled space below. This means that the gas breakthrough curves measured at different depths during experiment A

315 do not represent the transport conditions that would exist inside a continuous porous
316 medium, and fitted D_w values based on such data would therefore be incorrect. When
317 D_w is measured close to the surface exposed to wind, we recommend that the
318 samples used should be of sufficient thickness. The sensor should be installed at the
319 desired location inside the sample (such as in experiment B) rather than use thinner
320 samples with the sensor located at the bottom (such as in experiment A). Wind
321 turbulence penetration is likely to be proportional to air permeability of the porous
322 medium, k (Fukuda 1955), therefore values of D_w in porous materials with values of
323 k smaller than those used here can probably be measured with thinner samples than
324 we used without any loss of accuracy.

325 *Relation between wind-induced gas transport and distance to the surface exposed to*
326 *wind*

327 Values of D_w as a function of depth measured during experiment B for wind
328 conditions 1–12 are shown in Figure 5. The average coefficient of variation
329 (standard deviation divided by mean of the three replicates) across all data points in
330 Figure 5 is 1.24.

331

332 The D_w–z relations for all 12 wind conditions show similar patterns; D_w is
333 almost constant for z less than approximately10–15 cm. For $15 < z < 25$ cm. values
334 of D_w decrease relatively rapidly to near zero where they remain at larger depths.
335 This is different from the results of earlier theoretical modelling studies (Fukuda
336 1955; Massmann *et al*. 1997; Poulsen *et al.* 2001; Poulsen *et al.*, 2011) that assumed
337 an exponentially decreasing D_w–z relation. The results in Figure 5 suggest, therefore,

that assuming an exponential D_w–z relation when modelling wind-induced gas transport in porous media is possibly not completely correct. This is probably because earlier studies have assumed that wind velocities within the porous medium are one-dimensional and occur perpendicular to the surface exposed to wind only. Although net dispersive gas flux might still be represented as being one-dimensional, wind velocities are in reality likely to be multi-dimensional resulting in more complex D_w–z relations. Observed values of D_w in the upper 10–15 cm of the sample are between approximately 20 (for wind conditions 1–4) and 70 (for wind condition 12) times larger than D_m, which indicates that wind turbulence-induced gas transport in porous media under certain conditions can be more important than molecular diffusion.

Figure 5 further indicates that there is a tendency for D_w to increase with increasing values of vertical, horizontal and total wind velocity together with wind turbulence (standard deviations in Table 2 are an indicator of the intensity of wind turbulence) although the tendency is not fully consistent.

Figure 6a shows the breakthrough time (t_b) as a function of depth for the 13 wind conditions. In this case breakthrough time is taken as the amount of time that elapsed before the oxygen concentration at a given depth reaches 50% of its final value (10.5 relative to 21% oxygen). As expected, t_b increases with z (Figure 6a). Although t_b increases almost linearly with z for wind condition 0, the t_b–z relation is strongly non-linear for the remaining 12 wind conditions. Under windy conditions, t_b is very small for z less than about 15–20 cm and only increases for z > 20 cm. This corresponds well with the depth of penetration for the wind turbulence observed in

Figure 4. Oxygen breakthrough times are less for windy conditions than for the no wind condition for all depths investigated. Figure 6(a) also indicates a strong inverse relation between t_b and wind speed. The largest effect of wind turbulence on t_b occurs at shallow depths (z < 20 cm, Figure 6b). At these depths t_b under windy conditions is 2–9% only of the corresponding t_b values under calm conditions (molecular diffusion only). At larger depths the relative effect of wind on t_b decreases, however, at z = 30–35 cm wind effect still reduces t_b to between 23 and 55% of that observed under calm conditions. Note that breakthrough times at 2.5 cm were very small (Figure 6a), therefore, the values of relative breakthrough time at this depth were variable and not always physically meaningful. They were excluded therefore from Figure 6(b). The results in Figure 6 indicate that even though wind turbulence penetrates to a limited depth only, it can have a potentially large effect on gas transport at much larger depths.

Modelling D_w as a function of distance to the surface exposed to wind

Figure 5 indicates that the relations between D_w and z follow the same general pattern regardless of wind condition. To model relations with this pattern, Poulsen *et al*. (2006) suggested an expression based on the van Genutchen (1980) expression for soil-water retention. With the D_w–z relation this model takes the form:

$$\frac{D_w}{D_{w0}} = \frac{1}{(1+(\alpha z)^{\beta})^{\left(1-\frac{1}{\beta}\right)}}, \qquad (10)$$

where D_{w0} is the value of D_w at the surface of the porous medium and α and β are empirical constants. Best fitting curves for Equation (10) to the D_w–z and the D_w/D_{w0}–z relations using the fitting approach described above with D_{w0}, α and β as fitting parameters are shown in Figure 5 and Figure 7(a), respectively. Measured

383 values plotted against fitted values of D_w (with Equation (10)) are shown in Figure
384 7(b). Resulting values of D_{w0}, α and β are given in Table 2.
385
386 Figure 7(a,b) shows that Equation (10) can fit the experimental D_w values
387 closely, which indicates that it could potentially be used to represent the D_w–z
388 relation for modelling wind-induced gas transport in porous media. The amount of
389 experimental data used here is relatively small and is based on a single porous
390 medium; therefore, more data from a larger set of porous media with a wider range
391 of physical properties are needed to verify the applicability of Equation (10).
392 Figure 8 shows the relations between α and V_z (Figure 8a) and also α and β
393 (Figure 8b). V_z is average near-surface vertical wind speed. There is a weak inverse
394 relation between α and V_z, which indicates that, α depends to some degree on wind
395 conditions. Relations between α and other wind characteristics did not show any
396 strong trends. There is a relatively strong inverse relation between α and β, which
397 suggests further that β also depends on wind conditions. A direct correlation between
398 β and wind characteristics, however, did not reveal any strong trends, which suggests
399 that this relation is possibly more complex. Furthermore, it is likely that the relations
400 in Figure 8 are specific to the type of porous material used, therefore, more data are
401 required to assess if this is the case.
402

403 **Conclusions**

404 The results show that wind turbulence can potentially have a considerable effect on
405 gas dispersion in the porous medium and on gas exchange between the medium and

406 the atmosphere. For the wind conditions considered in this study, gas dispersion was
407 20–70 times greater than for calm conditions (molecular diffusion only) near the
408 surface of the porous medium exposed to wind. In addition, we observed that
409 although wind turbulence affects gas dispersion close to the surface exposed to wind
410 only (in this case 20 cm into the medium), it can have effects on the variation in gas
411 concentration at much greater depths. An increase in average wind speed and
412 fluctuations in wind speed and direction seemed to increase wind-induced transport
413 although the relation was not simple. To establish this relation, further experiments
414 with a wider range of wind conditions and properties of the porous medium than
415 considered here are needed.
416 The results indicate further that measurements with deeper samples and with
417 multiple gas sensors placed inside the sample are more reliable than for a series of
418 thinner samples with the gas sensor placed at the bottom. Measurements with deeper
419 samples equipped with multiple gas sensors are also much more rapid to carry out,
420 therefore, we suggest that this approach should be adopted for the measurement of
421 wind turbulence-induced gas transport.
422

References

Acharya, C.L. & Prihar, S.S. 1969. Vapor losses through soil mulch at different wind velocities. *Agronomy Journal*, **61**, 666–668.

Colbeck, S. C. 1981. A simulation of the enrichment of atmospheric pollutants in snow cover runoff. *Water Resources Research*, **17**, 1383–1388.

Denny, M.W. 1993. *Air and Water: The Biology and Physics of Life's Media*. Princeton University Press, Princeton, NJ.

Farrell, D.A., Greacen, E.L. & Gurr, C.G. 1966. Vapor transfer in soil due to air turbulence. *Soil Science*, **102**, 305–313.

Fukuda, H. 1955. Air and vapor movement in soil due to wind gustiness. *Soil Science*, **79**, 249–256.

Hanks, R.J. & Woodruff, N.P. 1958. Influence of wind on water vapor transfer through soil, gravel, and straw mulches. *Soil Science*, **86**, 160–164.

Ishihara, Y., Shimojima, E. & Harada, H. 1992. Water-vapor transfer beneath bare soil where evaporation is influenced by a turbulent surface wind. *Journal of Hydrology*, **131**, 63–104.

Kimball, B.A. & Lemon, E.R. 1970. Spectra of air pressure fluctuations at the soil surface. *Journal of Geophysical Research*, **75**, 6771–6777.

Kirkham, D. 1947. Field method for determination of air permeability of soil in its

undisturbed state. *Soil Science Society America Journal,* **11**, 93–99.

Maier, M., Schack-Kirchner, H., Aubinet, M., Goffi, S., Longdoz, B. & Parent,F. 2012. Turbulence effect on gas transport in three contrasting forest soils. *Soil Science Society of America Journal*, **76**, 1518–1528.

Massman, W.J. & Frank, J.M. 2006. Advective transport of CO2 in permeable media induced by atmospheric pressure fluctuations: 2. Observational evidence under snowpacks. *Journal of Geophysical Research: Biogeosciences*, **111**, G3

Massman, W.J., Sommerfeld, R.A., Mosier, A.R., Zeller, K.F., Hehn, T.J. & Rochelle, S.G. 1997. A model investigation of turbulence-driven pressure-pumping effects on the rate of diffusion of CO2, N2O and CH4 through layered snowpacks. *Journal of Geophysical Research*, **102**, 18 851–18 863.

Millington, R. & Quirk, J.P. 1961. Permeability of porous solids. *Transactions of the Faraday Society*, **57**, 1200–1207.

Nazaroff, W. W. 1992. Radon transport from soil to air. *Reviews of Geophysics*, **30**, 137–160.

Novak, M.D., Chen, W., Orchansky, A.L. & Ketler, R. 2000a. Turbulent exchange processes within and above a straw mulch. Part I: Mean wind speed and turbulent statistics. *Agricultural and Forest Meteorology*, **102**, 139–154.

Novak, M.D., Ketler, R., Chen, W. & Orchansky, A.L. 2000b. Turbulent exchange processes within and above a straw mulch. Part II: Thermal and moisture regimes. *Agricultural and Forest Meteorology*, **102**, 155–171.

Oertel, C., Matschullat, J., Zurba, K., Zimmermann, F. & Erasmi, S. 2016. Greenhouse gas emissions from soils—A review. *Chemie der Erde – Geochemistry*, **76**, 327–352.

M.A. Oliver, A.L. Khayrat 2001, A geostatistical investigation of the spatial variation of radon in soil, *Computers & Geosciences*, **27**, 939–957

Penman, H.L. 1940. Gas and vapor movements in the soil. I. The diffusion of vapors through porous solids. *Journal of Agricultural Science*, **30**, 437–462.

Poulsen, T.G., Christophersen, M., Moldrup, P. & Kjeldsen, P. 2001. Modeling lateral gas transport in soil adjacent to old landfill. *Journal of Environmental Engineering(ASCE)*, **127**, 145–153.

Poulsen, T.G. & Moldrup, P. 2006. Evaluating effects of wind-induced pressure fluctuations on soil-atmosphere gas exchange at a landfill using stochastic modelling. *Waste Management & Research*, **24**, 473–481.

Poulsen, T.G., Moldrup, P., Yoshikawa, S. & Komatsu, T. 2006. Bimodal probability law model for unified description of water retention, air and water permeability, and gas diffusivity in variably saturated soil. *Vadose Zone Journal*, **5**, 1119–1128.

480 Poulsen, T.G., Suwarnarat, W., Hostrup, M.K. & Kalluri, P.N.V. 2008. Simple and
481 rapid method for measuring gas dispersion in porous media: Methodology and
482 applications. *Soil Science*, **173**, 169–174.

483 Poulsen, T.G. & Sharma, P. 2011. Apparent porous media gas dispersion in response
484 to rapid pressure fluctuations. *Soil Science*, **176**, 635–641.

485 Riley, W.J., Robinson, A.L., Gadgil, A.J. & Nazaroff, W.W. 1999. Effects of
486 variable wind speed and direction on radon transport from soil into buildings: model
487 development and exploratory results. *Atmospheric Environment*, **33**, 2157–2168.

488 Russ, J.C. 2007. *The Image Processing Handbook, Fifth Edition*. CRC, Taylor &
489 Francis Group, Boca Raton, FL.

490 Saffman, P.G. 1960. Dispersion due to molecular diffusion and macroscopic mixing
491 in flow through a network of capillaries. *Journal of Fluid Mechanics*, **7**, 194–208.

492 Scotter, D.R. & Raats, P.A.C. 1968. Dispersion in porous mediums due to oscillating
493 flow. *Water Resources Research*, **4**, 1201–1206.

494 Scotter, D.R. & Raats, P.A.C. 1969. Dispersion of water vapor in soil due to air
495 turbulence. *Soil Science*, **108**, 170–176.

496 Takle, E.S., Brandle, J.R., Schmidt, R.A., Garcia, R., Litvina, I.V., Massman, W.J.*et*
497 *al*. 2003. High-frequency pressure variations in the vicinity of a surface CO2 flux
498 chamber. *Agricultural and Forest Meteorology*, **114**, 245–250.

499 Takle, E.S., Massman, W.J., Brandle, J.R., Schmidt, R.A., Zhou, X.H., Litvina,
500 I.V.*et al*. 2004. Influence of high-frequency ambient pressure pumping on carbon
501 dioxide efflux from soil. *Agricultural and Forest Meteorology*, **124**, 193–206.

502 Topp, E. & Pattey, E. 1997. Soils as sources and sinks for atmospheric methane.
503 *Canadian Journal of Soil Science*, **77**, 167–178.

504 van Genutchen, M.T. 1980. A closed-form equation for predicting the hydraulic
505 conductivity of unsaturated soils. *Soil Science Society of America Journal*, **44**, 892–
506 898.

507 Wang, F. & Ward, I.C. 2002. Radon entry, migration and reduction in houses with
508 cellars. *Building and Environment*, **37**, 1153–1165.

509

TABLE CAPTIONS

Table 1. Physical properties of the porous medium used in this study: d_{10} and d_{50} are the particle diameters for which 10% and 50% of the particles (by mass) are smaller, respectively, ϕ is total porosity, k is air permeability and ρ is particle roundness.

Table 2. Wind conditions used in the experiments in this study. V_z, V_x and V are near-surface vertical, horizontal and total wind speeds, respectively (average wind speed out and standard deviations in parentheses). The fitted values of D_{w0}, α and β from Equation (10) are also given.

519 Table 1

d_{10}/ mm	d_{50}/ mm	ϕ	k/ mm^2	ρ
6.7	8.5	0.29	0.18	0.75

520

521

522 Table 2

Wind condition	Average V_z	Average V_x /m s^{-1}	Average V	D_{w0} /m^2 s^{-1}	α	β
W0	0 (0)	0 (0)	0 (0)	-	-	-
W1	0.02 (0.43)	1.67(0.31)	1.73(0.31)	1.24(0.01)	0.06	34.24
W2	0.12(0.46)	1.80(0.36)	1.86(0.36)	1.10(0.05)	0.06	23.77
W3	0.13(0.46)	1.92(0.32)	1.98(0.32)	1.07(0.01)	0.06	23.98
W4	0.15(0.61)	1.98(0.39)	2.08(0.40)	1.04(0.02)	0.12	5.01
W5	0.30(0.75)	2.40(0.50)	2.53(0.52)	1.42(0.03)	0.09	4.36
W6	0.31(0.61)	2.33(0.46)	2.43(0.46)	2.51(0.04)	0.10	4.98
W7	0.36(0.60)	0.97(0.49)	1.19(0.50)	1.55(0.01)	0.05	18.16
W8	0.52(0.58)	2.74(0.42)	2.85(0.43)	1.58(0.07)	0.08	6.99
W9	0.66(0.60)	3.06(0.45)	3.19(0.47)	2.57(0.06)	0.07	12.10
W10	0.67(0.69)	3.27(0.54)	3.41(0.51)	2.80(0.07)	0.05	32.51
W11	0.83(0.59)	2.64(0.42)	2.83(0.42)	3.12(0.12)	0.06	12.75
W12	1.06(0.67)	1.55(0.63)	1.98(0.67)	3.43(0.03)	0.04	31.26

523

524

525

FIGURE CAPTIONS:

Figure 1. Schematic diagram of the experimental set-up. Cross-section of the equipment (left) and top view of the column (right). Schematic diagram is for set B experiments.

Figure 2. Variation in vertical (V_Z) and total (V) near surface wind speed as a function of time for wind condition W9 (Table 2).

Figure 3. Relative oxygen concentration (C/C_{atm}) as a function of time and depth for experiment B, under wind condition W3 where C_{atm} is the atmospheric oxygen concentration. Note that not all individual measurements (taken at 1s intervals) are shown.

Figure 4. Wind-induced dispersion coefficients (D_w) as a function of depth at wind conditions W3, W10 and W11 for: (a) Experiments type A and (b) Experiments type B.

Figure 5. Wind-induced dispersion coefficient, D_w, as a function of depth for wind conditions W1–W12. Symbols indicate D_w values measured during experiment B and curves are those that fitted best from Equation (10) to the measured data.

Figure 6. (a) Breakthrough time, t_b (time to reach 10.5% O_2), as a function of depth below the column surface for wind conditions W0–W12 and (b) relative breakthrough time (compared to wind condition 0) for wind conditions W1–W12. Note that the y-axis is reversed to represent measurement location better.

546 Figure 7. (a) D_w/D_{w0} as a function of depth for wind conditions 1–12. Symbols
547 indicate experimental values and curves are fitted by Equation (10) to the data and
548 (b) experimental values plotted against fitted values of D_w for wind conditions 1–12.

549 Figure 8. (a) Relation between vertical component of wind (V_z) and empirical
550 constant α and (b) relation between empirical constants α and β.

551

552

553

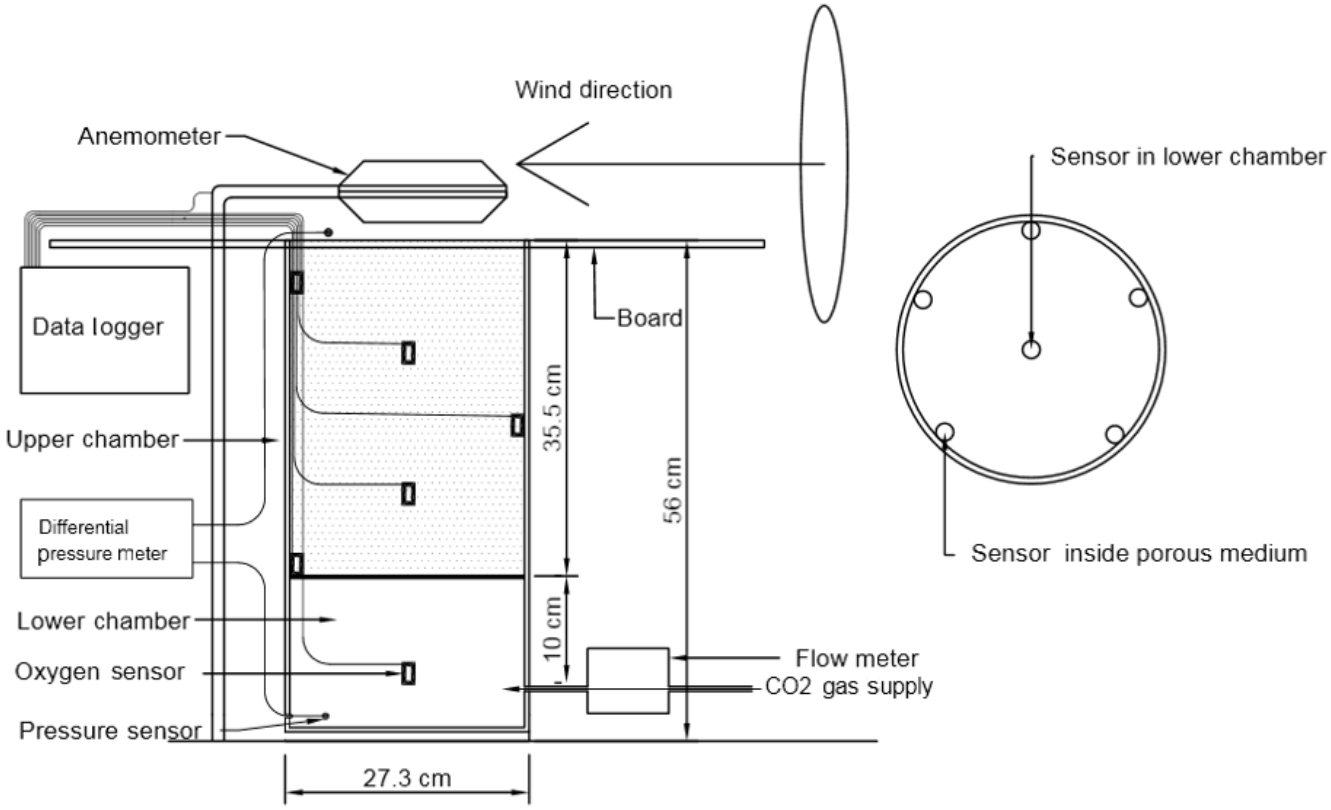

554
555 Figure 1.

556

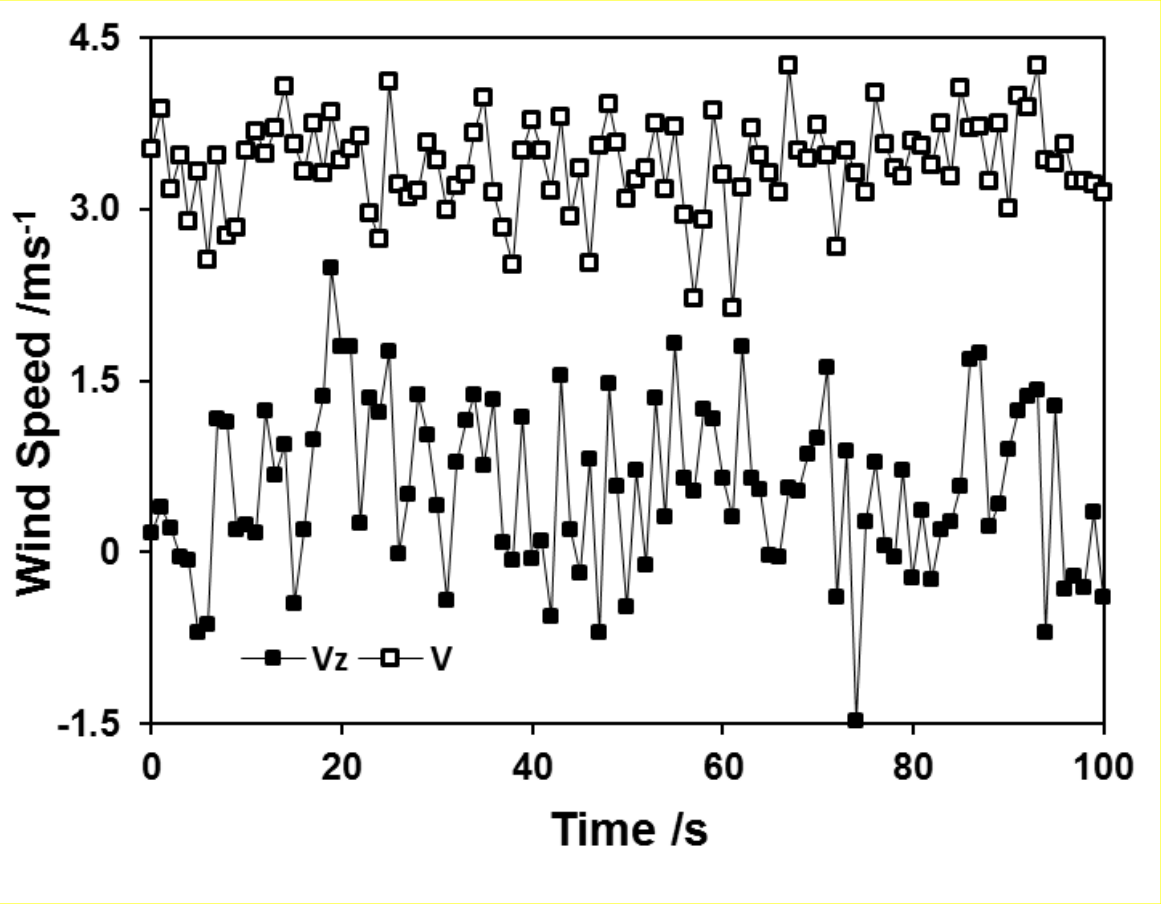

557

558 Figure 2.

559

560

561

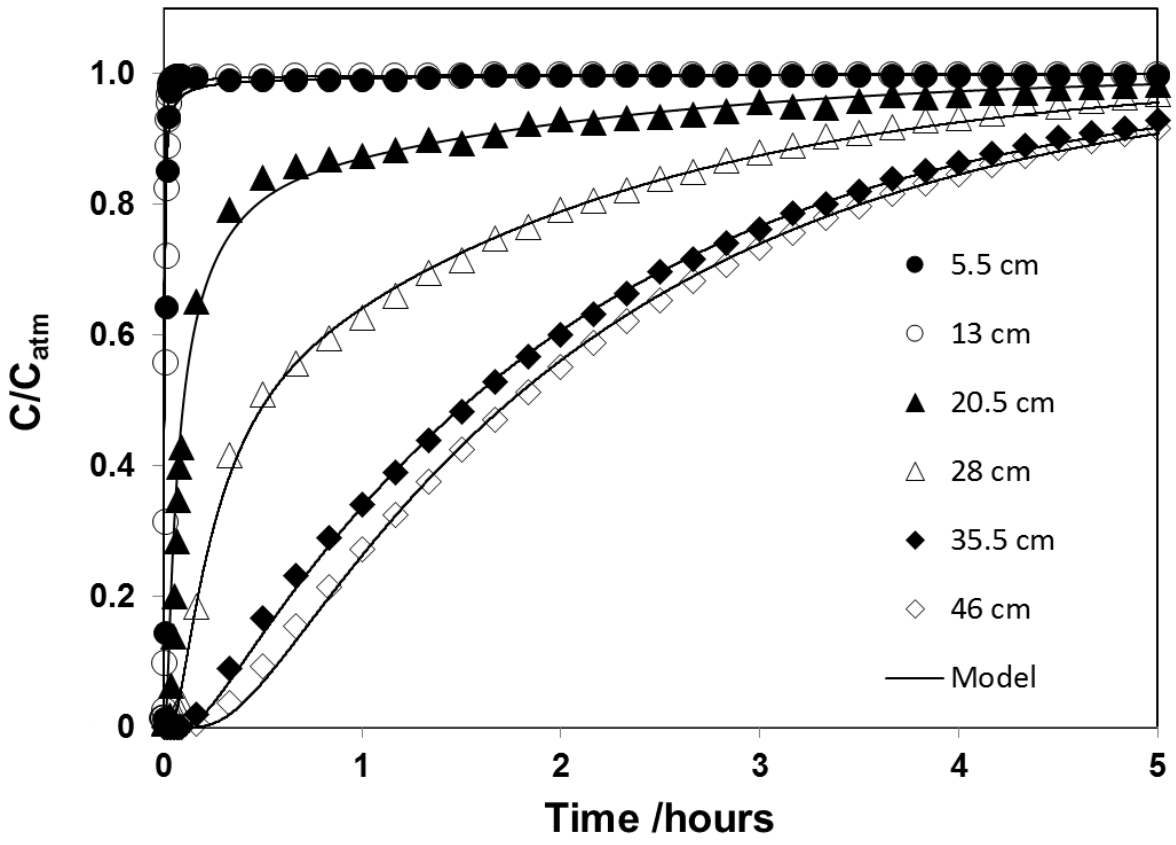

562

563 Figure 3.

564

565

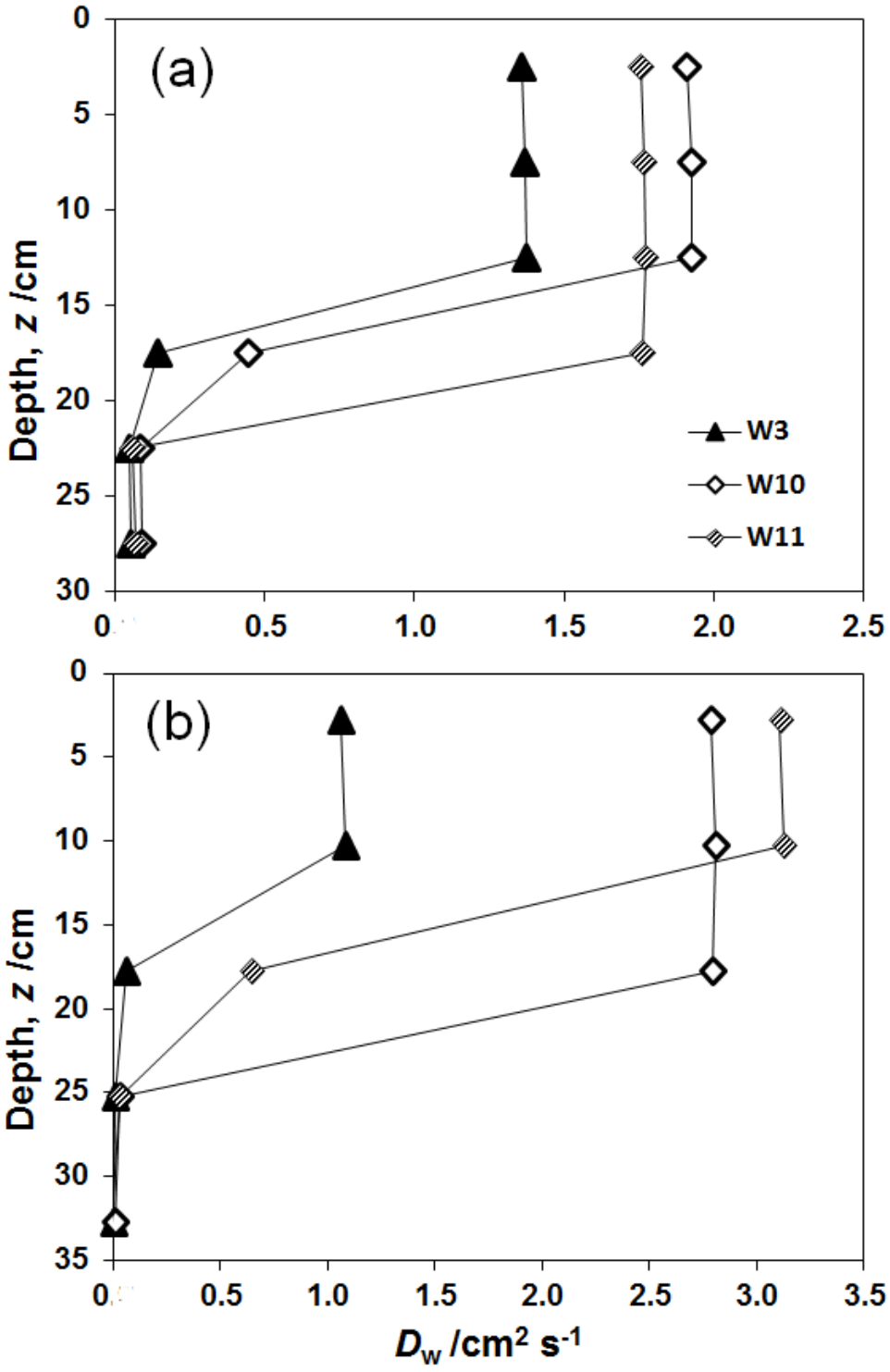

566

567 Figure 4.

568

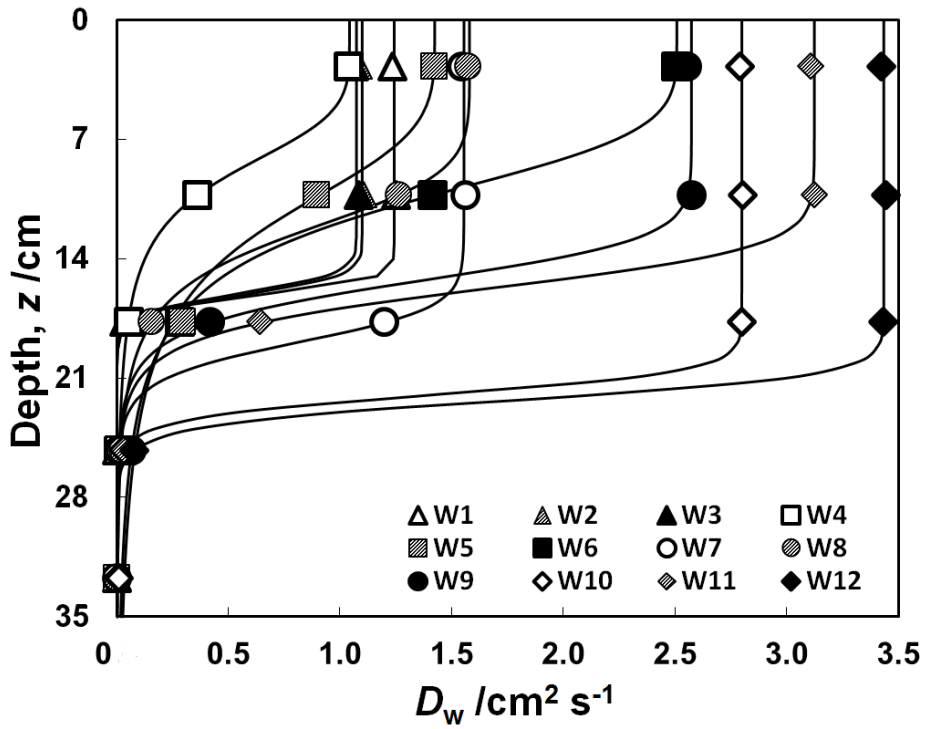

569

570 Figure 5.

571

572

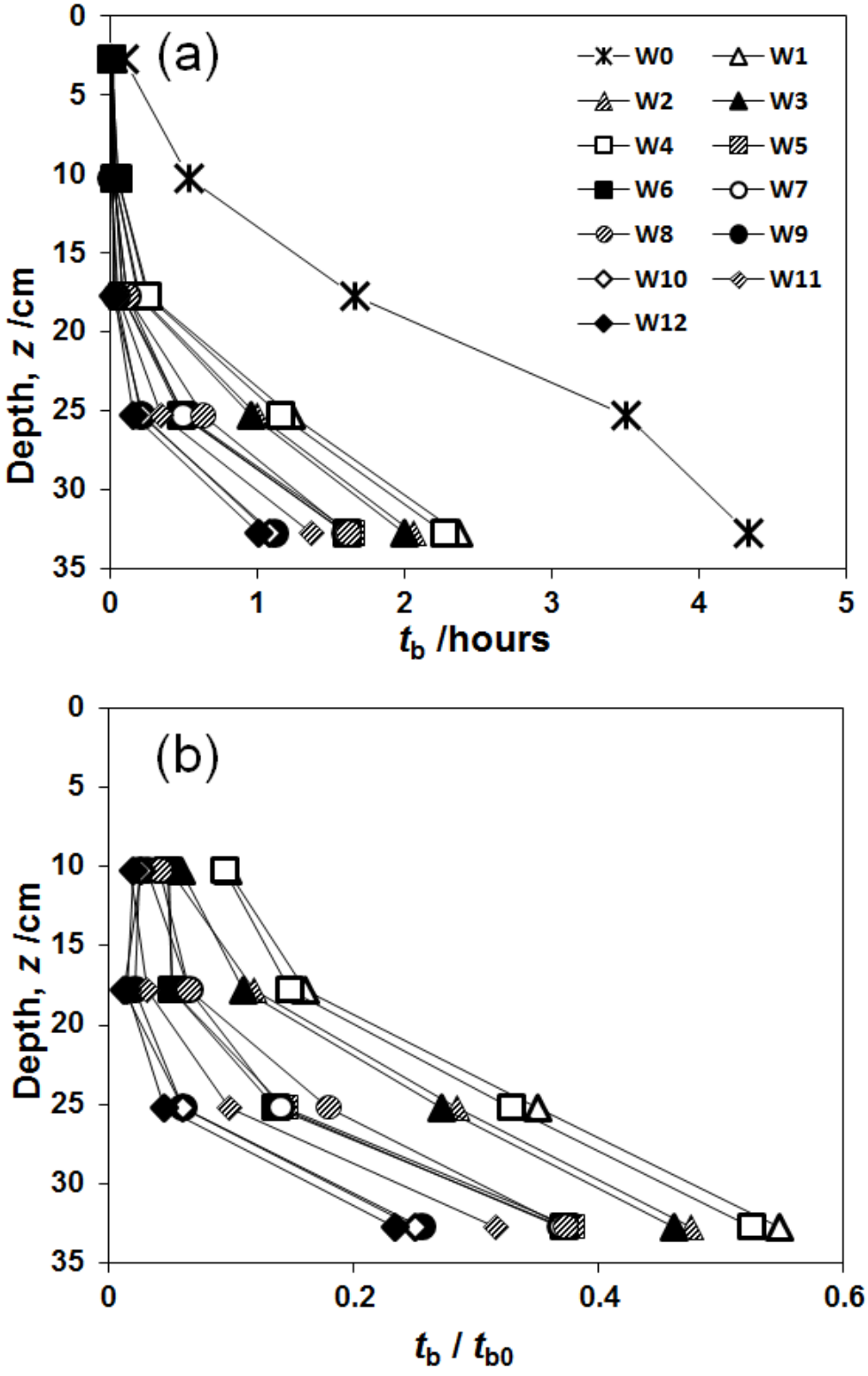

573

574 Figure 6.

575

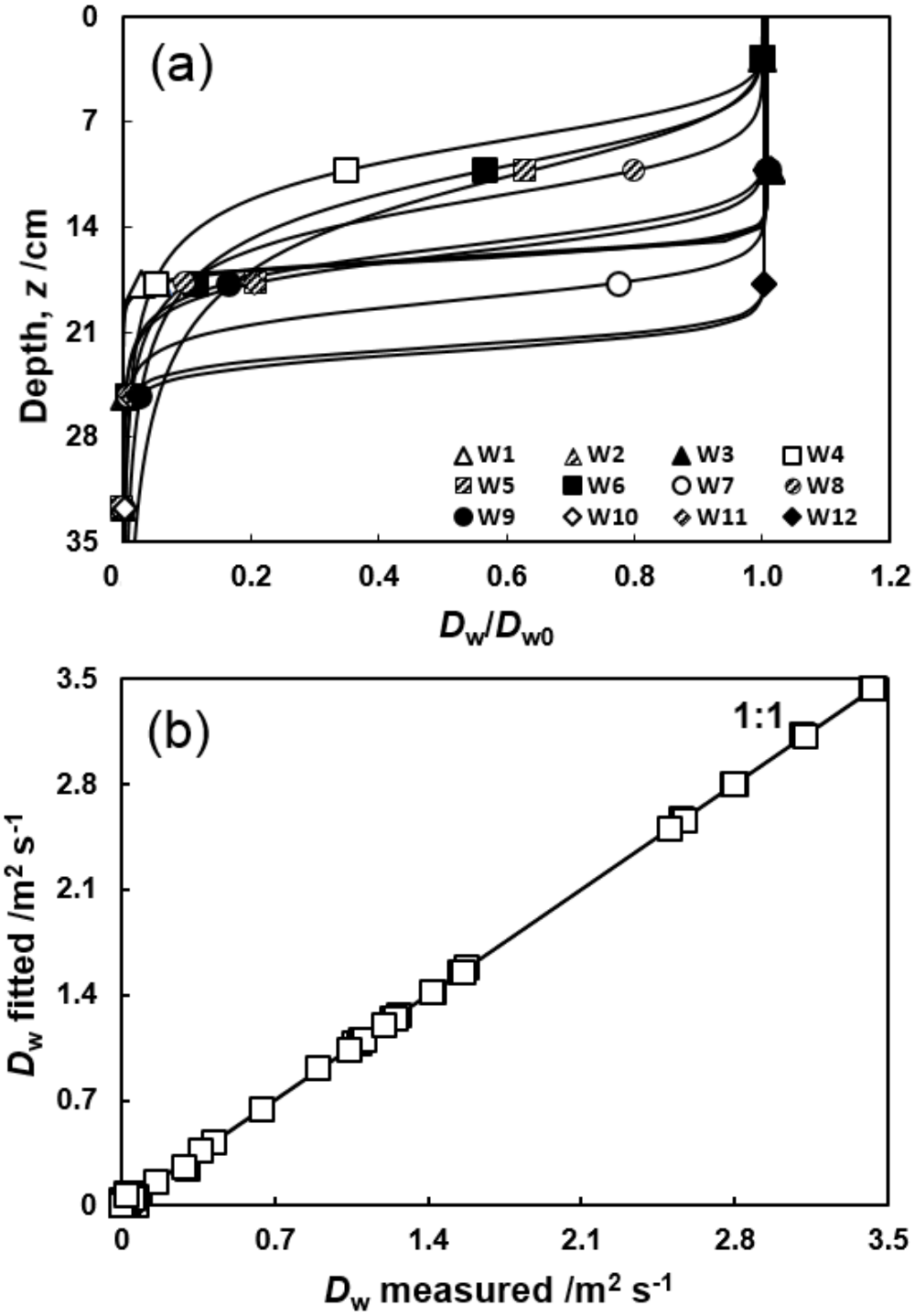
(a)
Depth, z /cm
0
7
14
21
28
35
0
0.2
0.4
0.6
0.8
1.0
1.2
D_w/D_{w0}
W1
W2
W3
W4
W5
W6
W7
W8
W9
W10
W11
W12
(b)
1:1
D_w fitted /m^2 s^{-1}
D_w measured /m^2 s^{-1}
0
0.7
1.4
2.1
2.8
3.5

Figure 7.

580

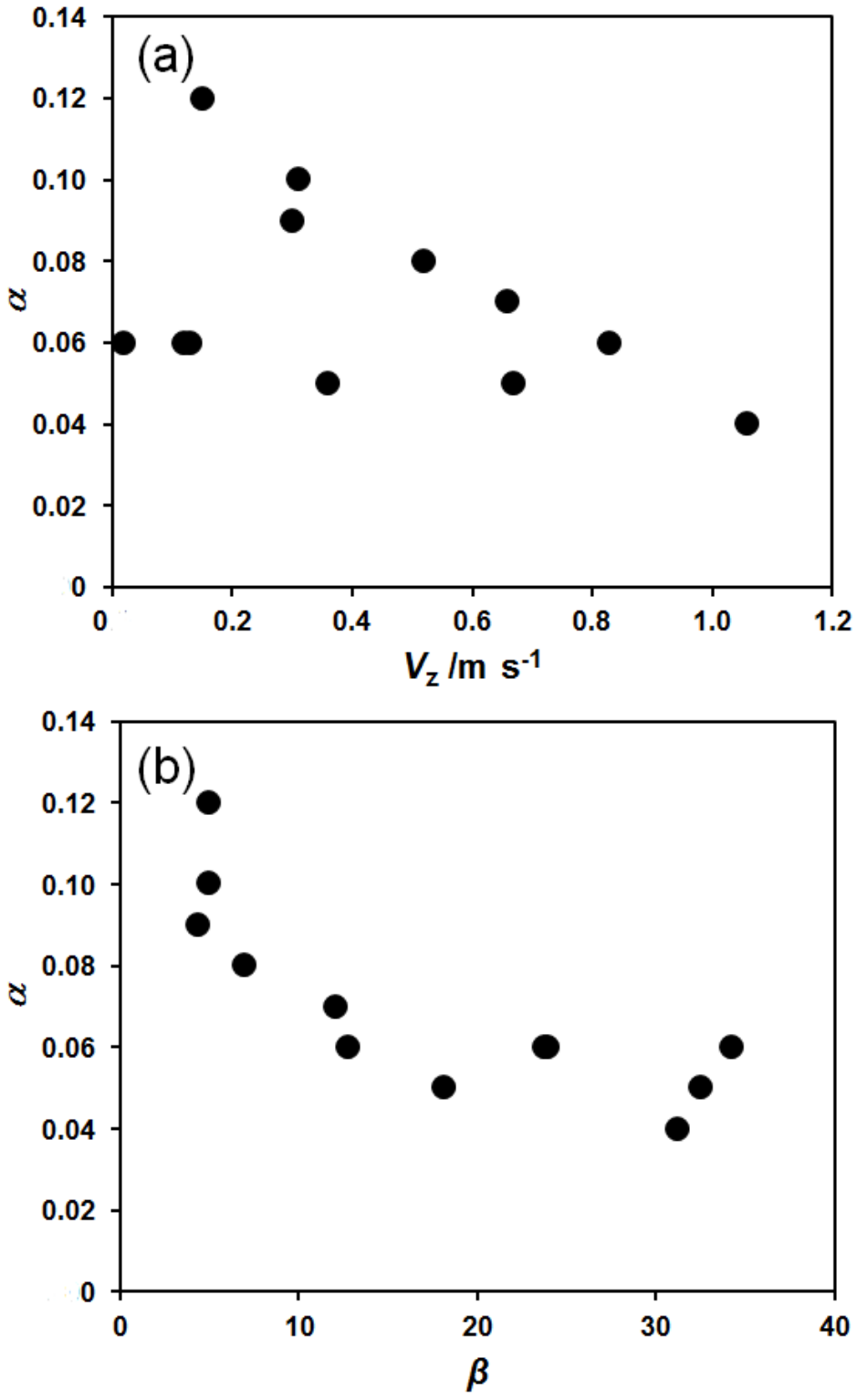

581

582 Figure 8.